JACS
JOURNAL OF THE AMERICAN CHEMICAL SOCIETY

Article

pubs.acs.org/JACS

Uniform, Dense Arrays of Vertically Aligned, Large-Diameter Single-Walled Carbon Nanotubes

Zhao Jun Han[†] and Kostya (Ken) Ostrikov*[,†,‡]

[†]Plasma Nanoscience Centre Australia (PNCA), CSIRO Materials Science and Engineering, Lindfield, New South Wales 2070, Australia

[‡]Plasma Nanoscience@Complex Systems, School of Physics, The University of Sydney, New South Wales 2006, Australia

Supporting Information

ABSTRACT: Precisely controlled reactive chemical vapor synthesis of highly uniform, dense arrays of vertically aligned single-walled carbon nanotubes (SWCNTs) using tailored trilayered Fe/Al_2O_3/SiO_2 catalyst is demonstrated. More than 90% population of thick nanotubes (>3 nm in diameter) can be produced by tailoring the thickness and microstructure of the secondary catalyst supporting SiO_2 layer, which is commonly overlooked. The proposed model based on the atomic force microanalysis suggests that this tailoring leads to uniform and dense arrays of relatively large Fe catalyst nanoparticles on which the thick SWCNTs nucleate, while small nanotubes and amorphous carbon are effectively etched away. Our results resolve a persistent issue of selective (while avoiding multiwalled nanotubes and other carbon nanostructures) synthesis of thick vertically aligned SWCNTs whose easily switchable thickness-dependent electronic properties enable advanced applications in nanoelectronic, energy, drug delivery, and membrane technologies.

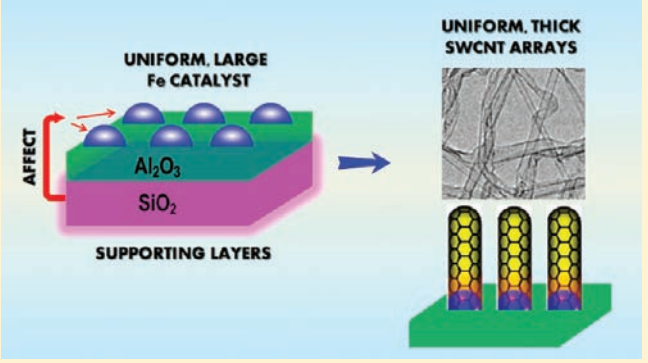

1. INTRODUCTION

Vertically aligned single-walled carbon nanotube (SWCNT) arrays have recently been a subject of considerable research activities owing to their unique mechanical, thermal, electrical, and optical properties. Owing to the enormous advantages of vertical alignment over random orientation, SWCNT arrays hold a great promise as building blocks in nanoelectronics, field emitters, light absorbers, drug delivery systems, gas sensors, water and molecular sieves, and energy storage devices, to mention just a few.[1−4] It is envisioned that the list of applications could become even wider if the morphology, length, and density of the arrays, as well as the diameter and chirality of individual SWCNTs inside the arrays, are precisely tailored.[5−7] However, such controlled growth has hitherto not been seen due to a lack of understanding of the growth mechanisms and the extreme sensitivity of SWCNT growth to the process conditions.[8−11]

Among a variety of parameters, the diameter of individual SWCNTs is of critical importance in determining the properties of SWCNT arrays. The diameter of SWCNTs is closely related to the energy band gap and the optical absorption of nanotubes (known as the Kataura plot).[12] For example, the energy band gap E_g of a semiconducting nanotube is inversely proportional to its diameter d_t, that is, $E_g = 4\gamma_b/3d_t$ (where γ_b is the band parameter).[13,14] Therefore, large-diameter SWCNTs possess a small energy gap that can facilitate the conversion from semiconducting to metallic, or from *p*- to *n*-type, through a simple and mild doping or using plasma procesings.[15] Large-diameter nanotubes are also beneficial in producing functional hybrid materials, miniaturized biomedical devices, as well as advanced platforms for nanotest-tube chemistry.[16−19] For these reasons, the preferential synthesis of large-diameter SWCNT arrays is highly warranted.

Presently, the most common and efficient method for synthesizing SWCNT arrays is chemical vapor deposition (CVD), which employs a catalyst (usually Fe, Co, or some bimetals) to decompose carbon-containing precursors and form nanotubes at high temperatures. Millimeter-long SWCNT arrays have been successfully grown in CVD processes by adding a trace amount of water as the catalyst preserver and growth enhancer (so-called "water-assisted CVD").[20] However, the direct synthesis of the uniform, dense arrays of large-diameter SWCNTs still remains a major challenge. Most of the previously reported surface-bound nanotubes synthesized in CVD processes have a diameter between 0.7 and 2 nm.[21−23] The vertically aligned nanotubes, on the other hand, possess a slightly larger diameter, ranging from 0.8 to 4 nm.[13,20,24−27] As large catalyst nanoparticles are generally considered to be less active in producing SWCNTs,[28,29] it is therefore extremely rare and difficult to synthesize vertically aligned SWCNTs with a diameter >5 nm. In addition, the role of catalyst supporting

Received: January 25, 2012
Published: March 12, 2012

   dx.doi.org/10.1021/ja300805s | *J. Am. Chem. Soc.* 2012, 134, 6018−6024

layers that have recently been very instrumental in the synthesis of SWCNT arrays has not been fully understood. These layers serve to prevent interlayer catalyst diffusion and facilitate the control of surface energy, which in turn affect the density and size distribution of catalyst nanoparticle and hence the growth of SWCNTs.[30,31] Despite many years of research efforts, it still remains unclear how to gainfully select and optimize the material and thickness of these supporting layers to enable effective control of SWCNT nucleation and growth.

In this work, we employ two trilayered $Fe/Al_2O_3/SiO_2$ catalyst systems and tackle the persistent issue of preferential synthesis of uniform, dense arrays of vertically aligned SWCNTs with a large diameter. By tailoring thickness and microstructure of the secondary catalyst supporting SiO_2 layer, we demonstrate that both the size and the number density of Fe catalyst nanoparticles can be effectively controlled. Consequently, thick nanotubes (>3 nm in diameter) nucleate and grow on the large catalyst nanoparticles while thin nanotubes and amorphous carbon are effectively etched away in the water-assisted CVD process. Our detailed microscopic analyses reveal that the nanotubes obtained in the present experiments have a mean diameter of 5−7 nm, with ∼34% in the diameter range of 7−10 nm and many larger than 10 nm, and only <5% are smaller than 3 nm. We propose (and subsequently validate through a series of extra experiments) a growth model that takes into account the commonly overlooked effect of the secondary supporting layer. The results suggest that this effect is critically important in the controlled synthesis of vertically aligned, large-diameter SWCNTs and the utilization of such materials in next-generation nanodevices for a large variety of applications.

2. RESULTS AND DISCUSSION

2.1. Morphological and Structural Analysis: Effect of Secondary Underlayer. Two catalyst systems with the same primary supporting layer but different secondary supporting layer were prepared to grow SWCNT arrays (Figure S1 of the Supporting Information). Specifically, **catalyst I** had the Fe thin film supported by a primary Al_2O_3 underlayer and a secondary SiO_2 underlayer; both were prepared using e-beam evaporation. On the other hand, **catalyst II** had the same Al_2O_3 underlayer but the secondary SiO_2 underlayer was prepared by thermal oxidation (Figure S1 of the Supporting Information). By annealing the two catalysts in an Ar/H_2 ambience to the desired growth temperature (750 °C), ethylene (C_2H_4) as the carbon feedstock and water vapor as the enhancer were introduced to start the growth of SWCNTs at atmospheric pressure. After a certain time (typically 10 min), C_2H_4 and water vapor were terminated, and the samples were cooled down to room temperature under the Ar gas flow.

A striking difference in the morphology and density of SWCNTs was found on the two catalysts when C_2H_4 was at 100 sccm and water vapor was carried by a 50 sccm Ar gas flow. Vertically aligned, densely packed arrays of SWCNTs appeared on **catalyst I** while randomly oriented, entangled nanotube networks were observed on **catalyst II**, as shown in Figure 1a and b, respectively (more images and the nanotubes grown without water are shown in Figure S2 of the Supporting Information). The resonant micro-Raman spectra of both samples probed at laser excitations of 514 and 633 nm are also presented in Figure 1c and d. The characteristic radial-breathing mode (RBM) in the low-frequency region (100−350 cm^{-1}) is clearly observed, indicating the existence of

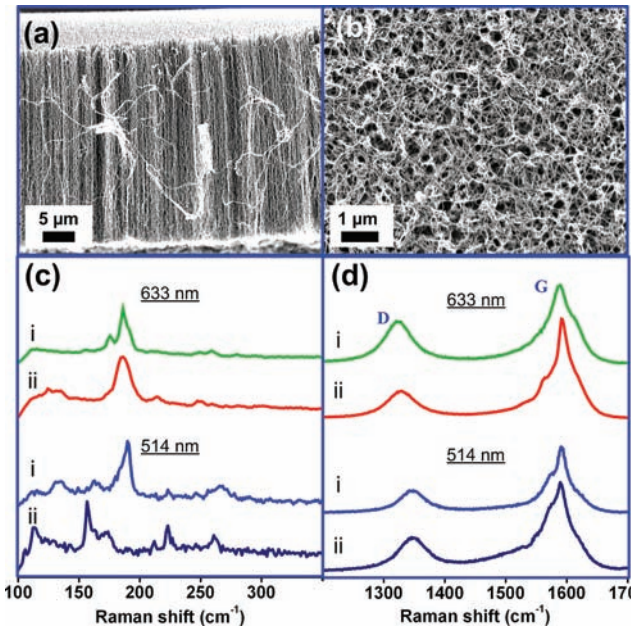

Figure 1. SEM images of (a) vertically aligned, densely packed SWCNTs grown on **catalyst I** and (b) entangled nanotube networks grown on **catalyst II**. Raman spectra at laser excitations of 514 and 633 nm of (c) radial-breathing mode (RBM) and (d) the D- and G-band modes of SWCNTs synthesized on (i) **catalyst I** and (ii) **catalyst II**.

SWCNTs. In fact, a pronounced portion of the RBM peaks was found in the 100−200 cm^{-1} range. As the frequency of RBM peaks ω_{RBM} is inversely proportional to the SWCNT diameter d_t, given by $\omega_{RBM} = 223.5/d_t + 12.5$,[32] the diameter of most grown nanotubes was therefore certainly larger than 1.5 nm. Furthermore, the tangential G-band and the defect-induced D-band Raman modes in the high-frequency region (1200−1700 cm^{-1}) are shown in Figure 1d. A relatively high D/G ratio, which is very common for the macroscopically sized SWCNT arrays synthesized by water-assisted CVD,[1,33] was observed for both samples. This could be an indication of water-induced imperfections in the graphitic walls of SWCNTs or the accumulation of carbonaceous impurities on the graphitic walls during the growth process.[34]

It is worth mentioning that, although the thickest nanotubes identifiable by the Raman spectroscopy are approximately 2 nm in diameter, SWCNTs with a larger diameter could certainly exist. Such nanotubes can be accurately analyzed and confirmed using other characterization techniques, in particular, transmission electron microscopy (TEM).[26,35−37] Figure 2 shows typical TEM images of SWCNTs grown on the two catalysts. Indeed, a common feature observed from these images is that most nanotubes were single-walled with a diameter larger than 3 nm. Multiple TEM images have also been collected; the corresponding histograms (total ∼300 nanotubes counted) indicated that a vast majority (>95%) of nanotubes synthesized on both catalysts were single-walled and more than 90% of these SWCNTs possessed diameters >3 nm (more TEM images see Figure S3 of the Supporting Information). In fact, we identified that the mean diameter of nanotubes was 5−7 nm, with ∼34% population in the diameter range of 7−10 nm and many larger than 10 nm, and only <5% were smaller than 3 nm (Figure 2). Atomic force microscopy (AFM) was also used to measure the diameter of SWCNTs dispersed in aqueous solutions, and the large diameter (>7 nm) of individual

dx.doi.org/10.1021/ja300805s | J. Am. Chem. Soc. 2012, 134, 6018−6024

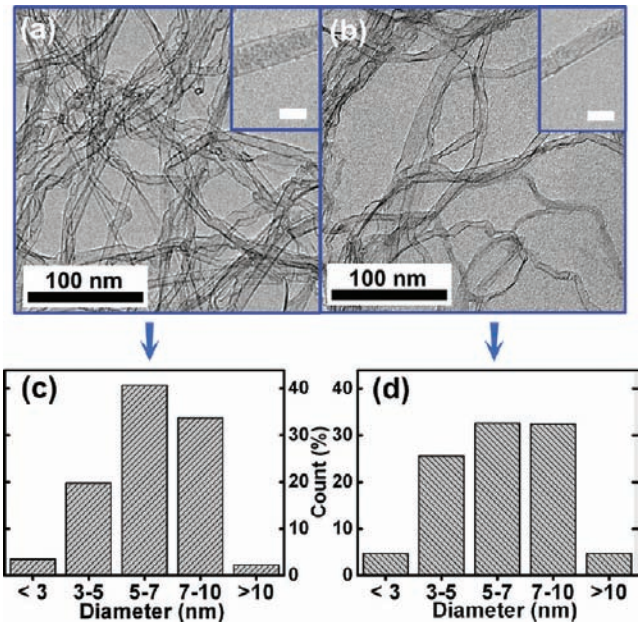

Figure 2. TEM images of SWCNTs grown on (a) **catalyst I** and (b) **catalyst II**. The insets are nanotubes identified with a diameter of ~10 nm. Scale bars in insets correspond to 10 nm. (c) and (d) are the histograms of nanotubes grown on **catalyst I** and **catalyst II**, respectively, showing that the nanotubes have a mean diameter of 5−7 nm, second largest population with 7−10 nm and many larger than 10 nm, and only <5% smaller than 3 nm, which are considerably larger than SWCNTs synthesized in the conventional CVD methods.

SWCNTs could be confirmed (see AFM and the line profiles in Figure S4 of the Supporting Information). These large-diameter SWCNTs have been rarely reported and are considerably larger than those obtained in other CVD processes.[13,20,24−27]

Thus, two features were unambiguously identified from the SWCNT arrays grown in water-assisted CVD: (i) the remarkable difference in the morphology and density of SWCNTs when using catalysts with different secondary supporting layers, and (ii) the prevalence of considerably larger-diameter nanotubes as compared to those produced in conventional thermal CVD processes (e.g., HiPco and CoMoCAT tubes have a mean diameter of 1.0 and 0.9 nm, respectively).[38,39] Very recently, Geohegan et al. obtained slightly smaller diameter (3−5 nm) SWCNT arrays in a low-pressure CVD process through adjusting the partial pressure of carbon feedstock.[35] They attributed such results to the suppression of nanotube nucleation on small catalyst nanoparticles that were overcoated by other carbon nanostructures.[35] Here, we stress that, since the process conditions were the same for the two catalysts in our case, the only possibility that led to the different structure of SWCNT arrays arose from the different secondary catalyst supporting layer. To understand how this secondary supporting layer affected the synthesis of SWCNTs arrays, a deeper understanding of the growth mechanism, particularly the nucleation of SWCNTs on catalyst nanoparticles, is imperative.

2.2. Catalyst Self-Organization. In general, three key mechanistic steps are involved in the growth of SWCNTs: nucleation, growth, and termination. Nucleation occurs when carbon species, dissociated from carbon-containing precursors at high temperatures, diffuse into/on the catalyst nanoparticles and segregate to form the initial carbon caps.[9] These caps usually follow the isolated pentagon rule and contain 5-fold carbon rings to facilitate the lift-off from the catalyst nanoparticles.[40] Recently, our numerical modeling indicated that, if the kinetic energy associated with the detachment of the carbon atoms from the catalyst nanoparticles is higher than the work of adhesion of the caps on the nanoparticles, the caps start to bend and lead to the growth of SWCNTs.[11] Furthermore, the growth of SWCNTs was also conceived as a reversible process at the catalyst nanoparticle sites.[41] It has been shown that the length of SWCNTs can be effectively controlled by the specific growth conditions.[42]

Clearly, the catalyst nanoparticles play a central role in the nucleation and growth of the nanotubes. Numerous experiments have evidenced that the diameter of SWCNTs is closely related to the size of catalyst nanoparticles.[43−47] In the current case, the formation of densely packed SWCNT arrays on **catalyst I** but not on **catalyst II** led us to assume that the size and number density of catalyst nanoparticles after pretreatment were different on the two samples. To validate this assumption, we have performed surface topological analyses on the catalysts undergoing the same pretreatment stage but not the nanotube growth stage. These catalysts were then fast-cooled to room temperature (5−7 °C/s) to largely preserve their crystalline structure, size, and shape.

The morphology of pretreated **catalysts I** and **II** revealed by AFM is shown in Figure 3a and b, respectively. As one can see in the figure, the number density of larger catalyst nanoparticles (height >3 nm) was significantly larger on **catalyst I** than that on **catalyst II**. Surface roughness analyses also indicated that the root-mean-square roughness (Rms) and the median height of catalyst nanoparticles on **catalyst I** were considerably larger

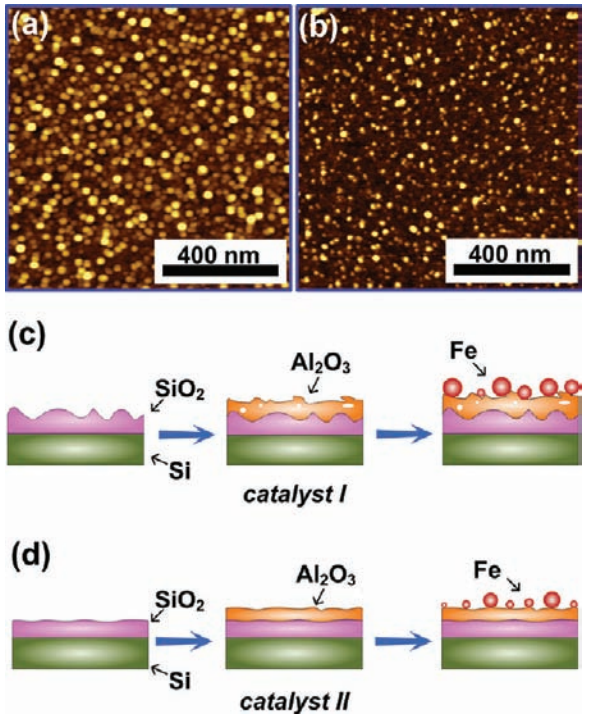

Figure 3. AFM images of (a) **catalyst I** and (b) **catalyst II** undergoing the pretreatment but not the growth stage. The brightest spots correspond to a height of 10 nm. Panels (c) and (d) show the schematics of how different secondary SiO_2 supporting layer affected the size and density of catalyst nanoparticles on **catalyst I** and **catalyst II**, respectively. Schematics in (c) and (d) are not to scale.

dx.doi.org/10.1021/ja300805s | J. Am. Chem. Soc. 2012, 134, 6018−6024

than those of **catalyst II** (Table S1 of the Supporting Information). This establishes a direct correlation between the number density of larger catalyst nanoparticles and the morphology and density of SWCNT arrays, by assuming that one larger catalyst nanoparticle supported one thicker nanotube.[43,44,47] To further understand why the secondary supporting layer can cause such a dramatic difference, we carefully analyzed the experimental conditions that led to the thermodynamic equilibrium of catalyst nanoparticles at high temperatures, as described in details below.

It is known that the size and shape of catalyst nanoparticles can be affected by a variety of controlling factors such as temperature, gas ambience, thickness of the original catalyst thin film, and catalyst–support interaction.[48−50] At elevated temperatures, thermodynamically stable catalyst nanoparticles are achieved by minimizing the surface free energy of the nanoparticles and the interfacial free energy between the nanoparticles and the supporting underlayer.[50,51] Since the temperature, gas ambience, and thickness of the original Fe thin films were identical in the current case, surface free energy of nanoparticles could hardly be the dominant factor that led to such a dramatic difference in the two catalysts. The most-likely factor was therefore related to the catalyst–support interaction, which is believed to be effective in modifying a variety of surface processes such as adatom diffusion, cluster migration and coalescence, as well as Ostwald ripening.[52−54]

In the Fe/Al_2O_3 catalyst system, the Al_2O_3 underlayer is used to maintain the structural order and reduce the surface diffusion when the Fe catalyst is fragmented into nanoparticles.[50] As compared to the Fe/SiO_2 catalyst, the strong interaction between Fe and Al_2O_3 can effectively produce a larger amount of active Fe nanoparticles, resulting in the growth of vertically aligned SWCNTs.[27] Indeed, many researchers observed that, when the catalyst was changed to Fe/SiO_2, it became very hard, if possible at all, to grow SWCNT arrays due to a lack of sufficiently active catalyst nanoparticles.[50,52] In addition, if surface properties of the Al_2O_3 underlayer are altered, the lifetime, activity, and coalescence of Fe catalyst nanoparticles could be strongly influenced. Amama et al. found that sputtered or e-beam deposited Al_2O_3 surfaces could introduce high void fractions into the deposited films, leading to a higher surface porosity and denser SWCNT arrays than on sapphire substrates.[30] Zhu and co-workers also indicated that Al_2O_3 deposited by ion-beam assisted deposition (IBAD) had a much longer catalyst lifetime and resulted in the synthesis of ultralong, spinnable CNT arrays.[55]

The same could occur on the secondary SiO_2 supporting layer used in our experiments when it was prepared by different methods. As compared to the flat thermally grown SiO_2 layer, a higher porosity and a large surface roughness were induced in the e-beam deposited SiO_2 layer. Subsequently, the thin Al_2O_3 supporting layer (10 nm) could be modified and render different surface morphology, porosity, and stress, arising from the trapped voids.[56,57] Our atomic force microanalyses and the optical reflectance measurements indeed demonstrated that, although the first Al_2O_3 supporting layer was prepared under the same conditions, the surface roughness and reflectance of the two catalysts appeared differently before thermal annealing (Figure S5 of the Supporting Information). Such differences arose from the different properties of the secondary SiO_2 supporting layers. Consequently, the Al_2O_3 layer affected the restructuring of Fe single crystals, resulting in different size, shape, and density of catalyst nanoparticles.[30,51,53] Ultimately, the morphology and density of grown SWCNT arrays were altered to a large extent.[8] Figure 3c and d are the schematic diagrams explaining the influence of the secondary supporting layers on **catalyst I** and **catalyst II**, respectively.

2.3. Effect of Reactive Chemical Etching. Besides the catalyst effect, the preferential synthesis of large-diameter SWCNTs is also closely related to the role of water vapor in the water-assisted CVD process. For a mixture of catalyst nanoparticles containing a variety of particle sizes, density functional theory (DFT) calculations showed that the heat of formation for nanotubes relative to that of graphene was reduced according to $1/d_t^2$ dependence,[58] suggesting that the formation of large-diameter nanotubes is more energetically favorable. However, the validity of such size dependence is limited to a critical value, beyond which the nucleation of nanotubes becomes difficult due to unstable caps and large work of adhesion.[11] Indeed, in most CVD processes where no water is present, multiwalled carbon nanotubes (MWCNTs) or carbon nanofibers are easily formed on large catalyst nanoparticles instead of large-diameter SWCNTs.[59−61] This is why, by merely increasing the thickness of a Fe catalyst film, it is not so straightforward to obtain arrays of large-diameter SWCNTs.

The etching effect of water molecules can suppress the nucleation of nanotubes on small nanoparticles. At the nucleation stage, SWCNT caps with a high curvature (i.e., on smaller nanoparticles) usually correspond to a larger strain and are more susceptible to the etching effect, while the caps with a low curvature (i.e., on larger nanoparticles) have a higher probability of survival.[37,62] Water molecules can also effectively remove additional graphitic layers on larger nanoparticles, which otherwise would result in the formation of multiwalled carbon nanotubes.[63] The combined effects of a high density of larger catalyst nanoparticles and water etching have therefore led to the prevalence of large-diameter SWCNTs, in consistent with our observations.

2.4. Further Supporting Experiments. To further corroborate the above analyses and gain more insight on how the secondary supporting layer affects the catalyst nanoparticles and ultimately the synthesis of SWCNT arrays, we carried out a series of complementary experiments using water-assisted CVD. First, we increased the C_2H_4 flow rate to 200 sccm with the constant concentration of water vapor. Quite similar results on the morphology and density of SWCNTs were obtained, that is, denser SWCNT arrays were grown on **catalyst I** but only "spaghetti-like" networks on **catalyst II** (Figure S6 of the Supporting Information). TEM images revealed that again these nanotubes had a large diameter. With an even higher C_2H_4 flow rate (600 sccm) and a prolonged growth time (40 min), ultralong (~120 μm) CNT arrays can be grown (Figure S7 of the Supporting Information). These macroscopically sized CNT arrays could easily detach from the growth substrate and are promising for the development of CNT-based membranes for water purification or electrodes for energy conversion and storage devices.[64] However, the type of nanotubes in these arrays had changed from single-walled to a mixture of both single- and few-walled nanotubes due to the increased carbon feed and the wall-thickening effect at a longer growth time (Figure S7 of the Supporting Information).[29,65]

Next, we adopted the "fast-heating" strategy to pretreat catalysts while other nanotube growth conditions remained the same. The "fast-heating" strategy is effective in creating much more active but smaller catalyst nanoparticles than in the normal heating process.[24,66] Interestingly, we found that, while

the vertical alignment of SWCNTs on **catalyst I** was about to form (thickness ~1 μm), there were only sparse nanotubes nucleated on **catalyst II** (Figure 4a and b). AFM images

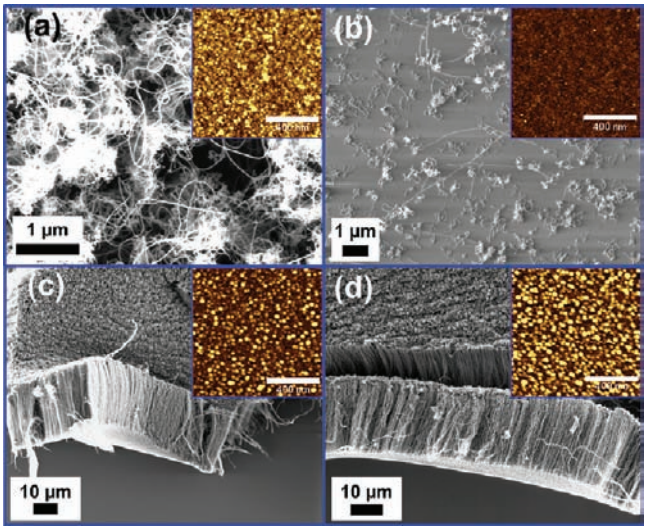

Figure 4. SEM images of SWCNTs synthesized in water-assisted CVD with the "fast-heating" pretreatment strategy on (a) **catalyst I** and (b) **catalyst II**. With a thicker Fe film of 1 nm, well-aligned SWCNT arrays were grown on both (c) **catalyst I** and (d) **catalyst II**. Insets are the corresponding AFM images for catalysts undergoing the pretreatment stage but not the growth stage. The brightest spots in these AFM images correspond to 4 nm in (a) and (b) and 10 nm in (c) and (d). Scale bar corresponds to 400 nm in all insets.

repeatedly showed that **catalyst I** had a higher density of large-sized nanoparticles than that of **catalyst II** (Table S1 of the Supporting Information), in a good agreement with the proposed SWCNT growth model.

Lastly, a thicker Fe layer (1 nm) of both underlayer configurations was used. As one can see in Figure 4c and d, vertically aligned SWCNT arrays were successfully grown on both catalysts this time. The corresponding AFM images indicated that, for a thicker Fe layer, the effect of the secondary supporting layer was minimized and the morphological difference in the two catalysts became indiscernible after pretreatment (the insets of Figure 4c and d). As a result, the grown SWCNT arrays had a similar morphology and density. These results therefore clearly demonstrate the applicability of the secondary underlayer configurations and that in general the size of catalyst nanoparticles indeed correlates with the morphology and density of the produced SWCNTs in the water-assisted process. Complemented with the presently available capability to control the electronic type (e.g., produce a large fraction of semiconducting SWCNTs in random networks[36]) of large-diameter single-walled nanotubes, our results are particularly important for the development of tailored arrays of (e.g., vertically aligned) SWCNTs for a large variety of applications.

More importantly, the additional advantage of our thick SWCNTs is that they have a small energy band gap. Hence, they can be easily made metallic by a simple processing, for example, acid or plasma doping.[15] Since $E_g = 4\gamma_b/3d_t$, the energy band gap for a semiconducting nanotube with a diameter of 1 nm is approximately 1.0 eV; while it is only 0.2 eV for a semiconducting nanotube with a diameter of 5−7 nm. These large-diameter nanotubes are thus particularly useful for the solution of a major challenge[3] of ultimately achieving arrays of all-metallic single-walled nantoubes.

3. CONCLUSIONS

In summary, we have demonstrated the preferential synthesis of uniform, dense arrays of vertically aligned, large-diameter (mean diameter of 5−7 nm, ~34% with the diameter of 7−10 nm and many larger than 10 nm, and only <5% are smaller than 3 nm) SWCNTs in water-assisted CVD. In contrast to many extensively studied processing parameters such as temperature, catalyst composition, and gas pressure, we have found that the secondary catalyst supporting layer could also play a major role in the growth of uniform arrays of vertically aligned SWCNTs. This secondary supporting layer effectively controlled both the size and the number density of Fe catalyst nanoparticles, which subsequently influenced the density, uniformity, and diameter of the grown SWCNTs in combination with the water etching effect. The growth model that took into account the hidden role of the secondary supporting layer explained the results from a series of experiments using different catalyst pretreatment conditions, different gas flow rates, and varied thickness of catalyst thin films. Our findings resolve the persistent issue of uniform arrays of vertically aligned, large-diameter single-walled carbon nanotubes. These results also hold promise for the improvement of catalytic synthesis of a large number of other one-dimensional nanostructures.

4. EXPERIMENTAL SECTION

The $Fe/Al_2O_3/SiO_2$ catalysts for synthesizing SWCNTs were prepared using two distinct methods. One was by sequentially depositing SiO_2 (100 nm thick), Al_2O_3 (10 nm thick), and Fe (0.5 or 1 nm thick) onto the *n*-type Si substrate (i.e., **catalyst I**); and the other was by depositing Al_2O_3 (10 nm thick) and Fe (0.5 or 1 nm thick) onto the *n*-type Si substrate with a 500 nm thick thermally grown oxide layer (i.e., **catalyst II**). All of the depositions were implemented using an electron-beam (e-beam) evaporator (Varian e-Gun). The thickness of all layers was monitored in situ by a quartz crystal microbalance and calibrated ex situ by a spectroscopic ellipsometer.

Vertically aligned SWCNTs were grown by water-assisted chemical vapor deposition (CVD) using C_2H_4 as the carbon feedstock and water as the catalyst preserver and growth enhancer.[20] Briefly, the prepared catalysts were loaded into a 2 in. quartz tube of a thermal furnace (MTI, OTF-1200). By purging with Ar for 15 min, the temperature of the thermal furnace was ramped to 750 °C in a mixture of Ar/H_2 (900/100 sccm) gases at atmospheric pressure. C_2H_4 (100−600 sccm) and water vapor carried by flowing Ar (20−200 sccm) into a water bubbler were then introduced. After a certain growth time (typically 10 min), C_2H_4, H_2, and water were terminated, and the samples were cooled down to room temperature under Ar gas flow.

The growth of SWCNTs with the "fast-heating" technique was implemented by quickly inserting the catalysts in an alumina boat into a preheated quartz tube held at the desirable temperature (750 °C). After dewetting the catalysts in the mixture of Ar/H_2 gases at atmospheric pressure for 5 min, the same growth and cooling conditions were used as above.

Field-emission scanning electron microscopy (FE-SEM) was performed using a Zeiss Ultra Plus microscope operated at 1 keV electron beam energy with an InLens secondary electron detector. Samples were viewed by scratching the surface with tweezers. Transmission electron microscopy (TEM) was performed using a Philips CM120 microscope equipped with an electron beam with the energy of 120 keV. The TEM samples were prepared by dispersing the grown nanotubes into ethanol and ultrasonicating for 30 min. The solution containing nanotubes was then placed onto holey carbon-coated copper grids and dried in air. Raman spectroscopy was performed using a Renishaw inVia spectrometer with two laser

excitations at 514 nm (Ar laser) and 633 nm (He−Ne laser) and a probing spot size of ∼1 μm^2. Atomic force microscopy (AFM) was performed using an Asylum Research MFP-3D microscope equipped with a Si cantilever (BudgetSensors). The cantilever had a spring constant of 5 N/m and a resonant frequency of 125 kHz. The tapping mode was adopted in all AFM scans.

■ ASSOCIATED CONTENT

Supporting Information

Surface roughness parameters of all AFM images shown in the main text, schematics of the two catalyst systems with the same primary supporting layer but different secondary supporting layer, SEM and TEM images of SWCNT arrays grown on the two catalysts, AFM and line profiles of large-diameter SWCNTs, surface roughness and reflectance of catalysts before thermal annealing and reduction, SEM images of SWCNT arrays grown with increased carbon feedstock, and the ultralong CNT arrays. This material is available free of charge via the Internet at http://pubs.acs.org.

■ AUTHOR INFORMATION

Corresponding Author

kostya.ostrikov@csiro.au

Notes

The authors declare no competing financial interest.

■ ACKNOWLEDGMENTS

The authors thank S. Dligatch for catalyst preparation, I. Levchenko, C. Fisher, and S. Yick for technical assistance and valuable discussions. Z.J.H. acknowledges CSIRO for the OCE Postdoctoral Fellowship. This work was partially supported by the Australian Research Council and CSIRO OCE Science Leadership Program.

■ REFERENCES

(1) Futaba, D. N.; Hata, K.; Yamada, T.; Hiraoka, T.; Hayamizu, Y.; Kakudate, Y.; Tanaike, O.; Hatori, H.; Yumura, M.; Iijima, S. *Nat. Mater.* **2006**, *5*, 987.

(2) Mizuno, K.; Ishii, J.; Kishida, H.; Hayamizu, Y.; Yasuda, S.; Futaba, D. N.; Yumura, M.; Hata, K. *Proc. Nat. Acad. Sci. U.S.A.* **2009**, *106*, 6044.

(3) Robertson, J.; Zhong, G.; Telg, H.; Thomsen, C.; Warner, J. H.; Briggs, G. A. D.; Dettlaff-Weglikowska, U.; Roth, S. *Appl. Phys. Lett.* **2008**, *93*, 163111.

(4) Han, Z. J.; Tay, B. K.; Tan, C. M.; Shakerzadeh, M.; Ostrikov, K. *ACS Nano* **2009**, *3*, 3031.

(5) Chiang, W.-H.; Sankaran, R. M. *Nat. Mater.* **2009**, *8*, 882.

(6) Ghorannevis, Z.; Kato, T.; Kaneko, T.; Hatakeyama, R. *J. Am. Chem. Soc.* **2010**, *132*, 9570.

(7) Volotskova, O.; Fagan, J. A.; Huh, J. Y.; Phelan, F. R. Jr.; Shashurin, A.; Keidar, M. *ACS Nano* **2010**, *4*, 5187.

(8) Zhang, G.; Mann, D.; Zhang, L.; Javey, A.; Li, Y.; Yenilmez, E.; Wang, Q.; McVittie, J. P.; Nishi, Y.; Gibbons, J.; Dai, H. *Proc. Nat. Acad. Sci. U.S.A.* **2005**, *102*, 16141.

(9) Han, Z. J.; Yick, S.; Levchenko, I.; Tam, E.; Yajadda, M. M. A.; Kumar, S.; Martin, P. J.; Furman, S.; Ostrikov, K. *Nanoscale* **2011**, *3*, 3214.

(10) Han, Z. J.; Levchenko, I.; Yick, S.; Ostrikov, K. *Nanoscale* **2011**, *3*, 4848.

(11) Ostrikov, K.; Mehdipour, H. *ACS Nano* **2011**, *5*, 8372.

(12) Kataura, H.; Kumazawa, Y.; Maniwa, Y.; Umezu, I.; Suzuki, S.; Ohtsuka, Y.; Achiba, Y. *Synth. Met.* **1999**, *103*, 2555.

(13) Oshima, Y.; Takenobu, T.; Yanagi, K.; Miyata, Y.; Kataura, H.; Hata, K.; Iwasa, Y.; Nojiri, H. *Phys. Rev. Lett.* **2010**, *104*, 016803.

(14) Ouyang, M.; Huang, J.-L.; Cheung, C. L.; Lieber, C. M. *Science* **2001**, *292*, 702.

(15) Zhang, J.; Wang, C.; Fu, Y.; Che, Y.; Zhou, C. *ACS Nano* **2011**, *5*, 3284.

(16) Singhal, R.; Orynbayeva, Z.; Sundaram, R. V. K.; Niu, J. J.; Bhattacharyya, S.; Vitol, E. A.; Schrlau, M. G.; Papazoglou, E. S.; Friedman, G.; Gogotsi, Y. *Nat. Nanotechnol.* **2011**, *6*, 57.

(17) Wu, J.; Paudel, K. S.; Strasinger, C.; Hammell, D.; Stinchcomb, A. L.; Hinds, B. J. *Proc. Nat. Acad. Sci. U.S.A.* **2010**, *107*, 11698.

(18) Hatakeyama, R.; Li, Y. F.; Kato, T. Y.; Kaneko, T. *Appl. Phys. Lett.* **2010**, *97*, 013104.

(19) Shiozawa, H.; Kramberger, C.; Pfeiffer, R.; Kuzmany, H.; Pichler, T.; Liu, Z.; Suenaga, K.; Kataura, H.; Silva, S. R. P. *Adv. Mater.* **2010**, *22*, 3685.

(20) Hata, K.; Futaba, D. N.; Mizuno, K.; Namai, T.; Yumura, M.; Iijima, S. *Science* **2004**, *306*, 1362.

(21) Picher, M.; Anglaret, E.; Arenal, R.; Jourdain, V. *ACS Nano* **2011**, *5*, 2118.

(22) Song, W.; Jeon, C.; Kim, Y. S.; Kwon, Y. T.; Jung, D. S.; Jang, S. W.; Choi, W. C.; Park, J. S.; Saito, R.; Park, C.-Y. *ACS Nano* **2010**, *4*, 1012.

(23) Kobayashi, K.; Kitaura, R.; Nishimura, F.; Yoshikawa, H.; Awaga, K.; Shinohara, H. *Carbon* **2011**, *49*, 5173.

(24) Xu, Y.-Q.; Flor, E.; Kim, M. J.; Hamadani, B.; Schmidt, H.; Smalley, R. E.; Hauge, R. H. *J. Am. Chem. Soc.* **2006**, *128*, 6560.

(25) Sundaram, R. M.; Koziol, K. K. K.; Windle, A. H. *Adv. Mater.* **2011**, *23*, 5064.

(26) Hasegawa, K.; Noda, S. *ACS Nano* **2011**, *5*, 975.

(27) Pint, C. L.; Alvarez, N. T.; Hauge, R. H. *Nano Res.* **2009**, *2*, 526.

(28) Li, Y.; Kim, W.; Zhang, Y.; Rolandi, M.; Wang, D.; Dai, H. *J. Phys. Chem. B* **2001**, *105*, 11424.

(29) Lu, C.; Liu, J. *J. Phys. Chem. B* **2006**, *110*, 20254.

(30) Amama, P. B.; Pint, C. L.; Kim, S. M.; McJilton, L.; Eyink, K. G.; Stach, E. A.; Hauge, R. H.; Maruyama, B. *ACS Nano* **2010**, *4*, 895.

(31) Fisher, C.; Han, Z. J.; Levchenko, I.; Ostrikov, K. *Appl. Phys. Lett.* **2011**, *99*, 143104.

(32) Bachilo, S. M.; Strano, M. S.; Kittrell, C.; Hauge, R. H.; Smalley, R. E.; Weisman, R. B. *Science* **2002**, *298*, 2361.

(33) Alvarez, N. T.; Pint, C. L.; Hauge, R. H.; Tour, J. M. *J. Am. Chem. Soc.* **2009**, *131*, 15041.

(34) Amama, P. B.; Pint, C. L.; McJilton, L.; Kim, S. M.; Stach, E. A.; Murray, P. T.; Hauge, R. H.; Maruyama, B. *Nano Lett.* **2009**, *9*, 44.

(35) Geohegan, D. B.; Puretzky, A. A.; Jackson, J. J.; Rouleau, C. M.; Eres, G.; More, K. L. *ACS Nano* **2011**, *5*, 8311.

(36) Yu, B.; Liu, C.; Hou, P.-X.; Tian, Y.; Li, S.; Liu, B.; Li, F.; Kauppinen, E. I.; Cheng, H.-M. *J. Am. Chem. Soc.* **2011**, *133*, 5232.

(37) Tian, Y.; Timmermans, M. Y.; Kivistö, S.; Nasibulin, A. G.; Zhu, Z.; Jiang, H.; Okhotnikov, O. G.; Kauppinen, E. I. *Nano Res.* **2011**, *4*, 807.

(38) Nikolaev, P.; Bronikowski, M. J.; Bradley, R. K.; Rohmund, F.; Colbert, D. T.; Smith, K. A.; Smalley, R. E. *Chem. Phys. Lett.* **1999**, *313*, 91.

(39) Bachilo, S. M.; Balzano, L.; Herrera, J. E.; Pompeo, F.; Resasco, D. E.; Weisman, R. B. *J. Am. Chem. Soc.* **2003**, *125*, 11186.

(40) Fan, X.; Buczko, R.; Puretzky, A. A.; Geohegan, D. B.; Howe, J. Y.; Pantelides, S. T.; Pennycook, S. J. *Phys. Rev. Lett.* **2003**, *90*, 145501.

(41) Crouse, C. A.; Maruyama, B.; Colorado, R. Jr.; Back, T.; Barron, A. R. *J. Am. Chem. Soc.* **2008**, *130*, 7946.

(42) Orbaek, A. W.; Owens, A. C.; Barron, A. R. *Nano Lett.* **2011**, *11*, 2871.

(43) Cheung, C. L.; Kurtz, A.; Park, H.; Lieber, C. M. *J. Phys. Chem. B* **2002**, *106*, 2429.

(44) Choi, H. C.; Kim, W.; Wang, D.; Dai, H. *J. Phys. Chem. B* **2002**, *106*, 12361.

(45) Li, N.; Wang, X.; Ren, F.; Haller, G. L.; Pfefferle, L. D. *J. Phys. Chem. C* **2009**, *113*, 10070.

(46) Ciuparu, D.; Chen, Y.; Lim, S.; Haller, G. L.; Pfefferle, L. *J. Phys. Chem. B* **2004**, *108*, 503.

(47) Ding, F.; Rosen, A.; Bolton, K. *J. Chem. Phys.* **2004**, *121*, 2775.

(48) Harutyunyan, A. R.; Chen, G.; Paronyan, T. M.; Pigos, E. M.; Kuznetsov, O. A.; Hewaparakrama, K.; Kim, S. M.; Zakharov, D.; Stach, E. A.; Sumanasekera, G. U. *Science* **2009**, *326*, 116.
(49) Lolli, G.; Zhang, L.; Balzano, L.; Sakulchaicharoen, N.; Tan, Y.; Resasco, D. E. *J. Phys. Chem. B* **2006**, *110*, 2108.
(50) Mattevi, C.; Wirth, C. T.; Hofmann, S.; Blume, R.; Cantoro, M.; Ducati, C.; Cepek, C.; Knop-Gericke, A.; Milne, S.; Castellarin-Cudia, C.; Dolafi, S.; Goldoni, A.; Schloegl, R.; Robertson, J. *J. Phys. Chem. C* **2008**, *112*, 12207.
(51) Wang, Y.; Luo, Z.; Li, B.; Ho, P. S.; Yao, Z.; Shi, L.; Bryan, E. N.; Nemanich, R. J. *J. Appl. Phys.* **2007**, *101*, 124310.
(52) Chakrabarti, S.; Kume, H.; Pan, L.; Nagasaka, T.; Nakayama, Y. *J. Phys. Chem. C* **2007**, *111*, 1929.
(53) Strongin, D. R.; Bare, S. R.; Somorjai, G. A. *J. Catal.* **1987**, *103*, 289.
(54) Ostrikov, K.; Levchenko, I.; Xu, S. *Pure Appl. Chem.* **2008**, *80*, 1909.
(55) Li, Q.; Zhang, X.; De Paula, R. F.; Zheng, L.; Zhao, Y.; Stan, L.; Holesinger, T. G.; Arendt, P. N.; Peterson, D. E.; Zhu, Y. T. *Adv. Mater.* **2006**, *18*, 3160.
(56) Zepeda-Ruiz, L. A.; Chason, E.; Gilmer, G. H.; Wang, Y.; Xu, H.; Nikroo, A.; Hamza, A. V. *Appl. Phys. Lett.* **2009**, *95*, 151910.
(57) Shim, Y.; Borovikov, V.; Uberuaga, B. P.; Voter, A. F.; Amar, J. G. *Phys. Rev. Lett.* **2008**, *101*, 116101.
(58) Li, Y.; Peng, S.; Mann, D.; Cao, J.; Tu, R.; Cho, K. J.; Dai, H. *J. Phys. Chem. B* **2005**, *109*, 6968.
(59) Yamada, T.; Nama, T.; Hata, K.; Futaba, D. N.; Mizuno, K.; Fan, J.; Yudasaka, M.; Yumura, M.; Iijima, S. *Nat. Nanotechnol.* **2006**, *1*, 131.
(60) Chiang, W.-H.; Futaba, D. N.; Yumura, M.; Hata, K. *Carbon* **2011**, *49*, 4368.
(61) Patole, S. P.; Kim, H.; Choi, J.; Kim, Y.; Baik, S.; Yoo, J. B. *Appl. Phys. Lett.* **2010**, *96*, 094101.
(62) Zhu, L.; Sun, Y.; Hess, D. W.; Wong, C.-P. *Nano Lett.* **2006**, *6*, 243.
(63) Kumar, S.; Levchenko, I.; Ostrikov, K.; McLaughlin, J. A. *Carbon* **2011**, *49*, 325.
(64) Ci, L.; Manikoth, S. M.; Li, X.; Vajtai, R.; Ajayan, P. M. *Adv. Mater.* **2007**, *19*, 3300.
(65) Cui, X.; Wei, W.; Chen, W. *Carbon* **2010**, *48*, 2782.
(66) Qu, L.; Du, F.; Dai, L. *Nano Lett.* **2008**, *8*, 2682.